

# Effect of Crystalline Structure on Intergranular Failure During Shock Loading

J.P. ESCOBEDO,<sup>1,3</sup> E.K. CERRETA,<sup>2</sup> and D. DENNIS-KOLLER<sup>2</sup>

1.—The University of New South Wales, Canberra BC, ACT 2610, Australia. 2.—Los Alamos National Laboratory, Los Alamos, NM 87544, USA. 3.—e-mail: j.escobedo-diaz@adfa.edu.au

The effect of crystalline structure on intergranular failure during shock loading has been examined. A suite of dynamic tensile experiments, using plate-impact testing, were conducted on copper (face-centered cubic) and tantalum (body-centered cubic) specimens with different grain sizes (30–200  $\mu\text{m}$ ). These experiments were designed to probe void nucleation, growth, and coalescence processes that for these materials are known to lead to failure. For the grain sizes examined in the study, post-impact metallographic analyses show that in copper specimens, during the early stages of deformation, voids were present primarily at general or low-coincidence, high-angle grain boundaries (GBs), irrespective of grain size. In tantalum, while some voids developed along the GBs, an increasing amount of transgranular damage was observed as the grain size increased. A scenario based on the availability of potential nucleation sites and number of slip systems inherent to each crystalline structure is discussed. The role that this availability plays in either promoting or hindering plastic processes leading to damage nucleation and growth is then examined.

## INTRODUCTION

There has been a need to gain a fundamental understanding of failure mechanisms in materials subjected to extreme conditions of high strain rates and stresses for a variety of applications. For instance, elucidating the failure mechanisms under such loading conditions may help military efforts in designing better defensive armor against projectile penetration, as well as aid the automotive industry endeavors for developing energy-absorbent structures during high-speed crash.

One methodology widely used to investigate material response under both high strain rate and stress is shock loading the material via controlled plate-impact experiments.<sup>1–4</sup> These experiments consist of an impactor launched against a sample target (Fig. 1a). This subjects a region within the material to a high tensile stress state on the order of few GPa. If the stress is high enough, then the material ultimately fractures.<sup>2,4–6</sup> This type of fracture has been normally referred to as spall.<sup>2,4,7</sup> The pioneering studies on this subject date back to the classic works carried out in the 1970s at the Stanford Research Institute (SRI) by Curran et al.<sup>4</sup>

and Seaman et al.,<sup>6</sup> followed by many studies ever since.<sup>1,5,7–18</sup> It has been shown that failure or spall fracture is a complex process strongly influenced by both the microstructure and the dynamic loading profile or shock wave shape imparted to the specimen. In ductile metals, these works have shown also that fracture occurs via a time-dependent damage process that involves the nucleation, growth, and coalescence of voids. These voids have been shown to nucleate preferentially at the interfaces of heterogeneities within the material.<sup>1–4,7,8,10,12,15–18</sup> For high-purity materials, these interfaces typically correspond to grain boundaries (GBs), which are the principal microstructural features addressed in this article.

Due to the complexity of the fracture process, it is necessary to decouple the two aspects of microstructure and loading kinetics. Recent work has addressed this problem and has aimed to accurately determine the individual contributions of microstructure and loading profile to the mechanisms responsible for damage development.<sup>17–20</sup> To this end, the emphasis has been on tracking the microstructural evolution at early stages of damage using copper as a model material—where it is still possible

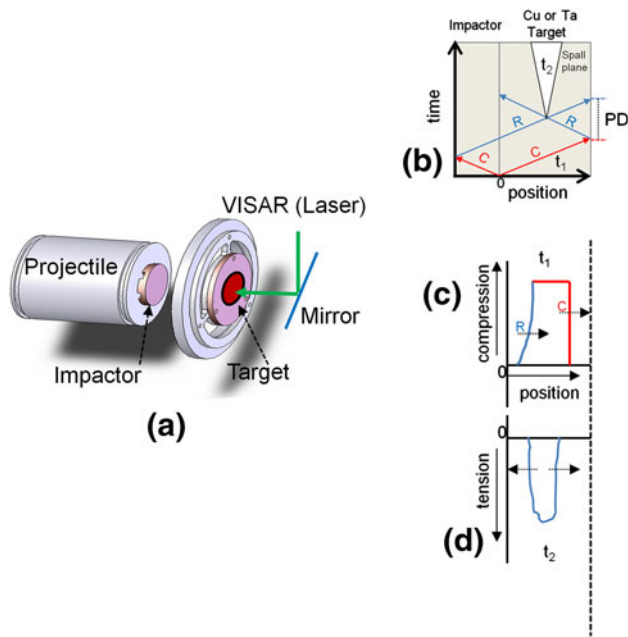


Fig. 1. Schematics showing (a) experimental configuration of a typical plate-impact experiment and (b) the  $x-t$  diagrams of the trajectory and interaction of compressive (C, colored as red) and release (R, colored as blue) waves, as well as the development of (c) compressive and (d) tensile pulses (Color figure online).

to link damage to initial microstructure of the undeformed material. For this reason, experiments were conducted at 1.5 GPa, a relatively low stress such that the damage fields correspond to incipient damage states, i.e., a full fracture plane has not yet formed. The most salient results of the microstructural effects on the mechanisms for damage evolution in copper recently reported in the literature<sup>18</sup> are as follows:

- (1) *Void nucleation* For all microstructures analyzed, damage is observed to develop preferentially along specific GBs with misorientation angle in the  $10^{\circ}$ – $57^{\circ}$  range. Significantly less damage was observed at the special, high-coincidence  $\Sigma 3$  GBs, which had crystallographic orientations on either side of the boundary similar to other high-angle boundaries that failed.<sup>17</sup> These results suggest that the structure of the interface determines the preferred location for void nucleation. Of special interest is that null or negligible damage was observed within grains.
- (2) *Void growth and coalescence* The least damage content was observed in microstructures with an average intermediate grain size in the 60–100  $\mu\text{m}$  range. Greater damage content was observed in samples with relatively small (30  $\mu\text{m}$ ) or large grain size (200  $\mu\text{m}$ ). These results suggest a length scale dependency for damage evolution. In addition, more recent work has shown that the material properties between two nucleated voids can promote or

hinder plastic deformation, in turn dictating void growth and coalescence.<sup>17,21</sup>

In this article, we build on the previous findings and investigate the role of crystalline structure on the damage evolution in body-centered cubic (bcc) tantalum and compare our results to those reported for face-centered cubic (fcc) copper. In this way, the role of crystallography on early stage dynamic damage is investigated. To this end, we conducted a suite of plate-impact experiments using high-purity tantalum with three different grain boundary densities and distributions. As we assess the individual role of internal interfaces (i.e., GBs) on damage evolution, we imposed similar loading profiles on all Ta samples. This was achieved by using 2-mm-thick quartz impactors, similar to the study on copper. The damage fields are characterized by means of optical and electron backscatter diffraction (EBSD) microscopy to gain a more comprehensive understanding of microstructural and damage evolution. The approach followed herein is an attempt toward understanding the role of the different microstructural aspects on materials performance in extreme conditions and a part of the initial steps for tailored design of damage-tolerant materials.

## EXPERIMENTAL METHODS

The plate-impact experiment consists of a single monolithic flyer mounted on a projectile launched against a sample target (Fig. 1a). On impact, an initial shock compressive state is generated in the sample for durations on the order of less than a microsecond, as indicated by the pulse duration (PD) in Fig. 1b and c. Then, as the sample decompresses from the shocked state, release waves travel from the free surfaces toward the interior of the target (blue lines in Fig. 1b). Their interaction results in the creation of tensile stresses in the interior of the specimen (Fig. 1d). The real-time, submicrosecond response is assessed by measurement of the free surface velocity of the target. This task can be performed by means of velocimetry interferometer for any surface reflector (VISAR)<sup>22</sup> or photon Doppler velocimetry (PDV)<sup>23,24</sup> probes mounted  $90^{\circ}$  off of the shock direction axis to prevent any subsequent impact of the target with the probe. Then, by use of the Hugoniot equation of state of the specific material being studied, the mechanical state, i.e., stress, can be extracted. Additional experimental details can be found in Refs. 1,5,7,12,18, and 25.

In preparation for the plate-impact experiments, targets of the material of interest were fabricated as circular disks 15 mm in diameter and 4 mm in thickness. Materials of interest for this study were high-purity 99.999% Cu and high-purity Ta. The samples were annealed under vacuum at several temperatures and times to produce a set of microstructures with varying grain boundary distribution. Table I lists the annealing treatments as well

**Table I. Processing parameters for copper and tantalum microstructures**

Material	Heat treatment		Average grain size ( $\mu\text{m}$ ) <sup>a</sup>
	Temperature ( $^{\circ}\text{C}$ )	Time (min)	
Copper	450	30	30
Copper	850	60	80–100
Copper	925	30	200
Tantalum	As received (annealed)		35
Tantalum	1300	180	85
Tantalum	1500	60	200

<sup>a</sup>For copper, the reported grain size is without twins.

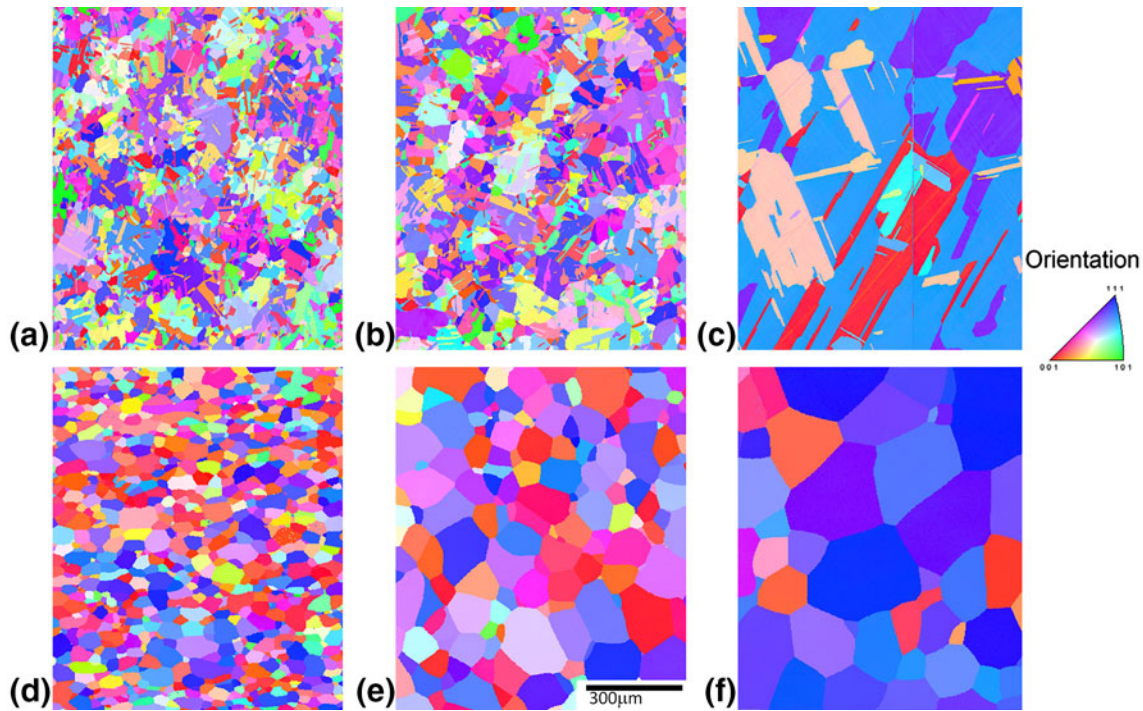


Fig. 2. Orientation maps of the annealed microstructures utilized in this study: copper grain size measured without twins: (a)  $\sim 30 \mu\text{m}$ , (b)  $\sim 100 \mu\text{m}$ , (c)  $\sim 200 \mu\text{m}$ ; and tantalum (d)  $\sim 35 \mu\text{m}$ , (e)  $\sim 85 \mu\text{m}$ , (f)  $\sim 200 \mu\text{m}$ . The weak 111 textures are typical and expected for annealed copper and tantalum.

as the average grain size for each microstructure tested in this study. Representative micrographs of the microstructures are shown in Fig. 2. The grain size is estimated by using the automated analysis for EBSD data in which twin boundaries are not included for the case of copper.

A group of representative experiments conducted in this study is listed in Table II. The experiments were conducted at peak compressive stresses of 1.5 GPa for copper and 5.7 GPa for tantalum. These stresses are just above the stress reported as the threshold for damage initiation for each material,  $\sim 1.3$  GPa for Cu<sup>17,18</sup> and  $\sim 5.2$  GPa for Ta.<sup>26–28</sup> For all experiments, *z*-cut quartz flyers were used to impose a similar shock wave loading profile on the Cu and Ta targets, respectively. After impact, each

recovered specimen was diametrically sectioned and mounted such that the cross section of the damaged sample was exposed for postimpact characterization. The deformed specimens were prepared following standard metallographic techniques up to a 0.05-mm colloidal silica final polish, performed on a vibratory polisher. Finally, the Cu samples were electropolished using a solution of two parts of phosphoric acid to one part of water at  $\sim 1.9$  V for  $\sim 10$  s. The Ta samples were chemically polished using a solution of 10 mL of sulfuric acid, 10 mL of nitric acid, and 5 mL hydrofluoric acid. Optical microscopy was performed on a Zeiss microscope (Carl Zeiss, Oberkochen, Germany) equipped with an automated stage. EBSD analysis was performed on a Philips XL30 field emission scanning electron microscope (FESEM);

**Table II. Parameters for plate-impact experiments**

ID	Impactor velocity (m/s)	Target thickness (mm)	Grain size ( $\mu\text{m}$ )	Compressive stress (GPa)	Damage $A_{\text{void}}/A$ (%)
Cu.1	134	4.0	30	1.5	0.496
Cu.2	133	4.0	100	1.5	0.281
Cu.3	131	4.0	200	1.5	0.510
Ta.1	409	4.0	35	5.7	0.163
Ta.2	404	4.0	85	5.7	0.370
Ta.3	409	4.0	200	5.7	0.425

All experiments were conducted using 2.0-mm-thick quartz impactors. The last column reports the damage in the form of void area fraction (%).

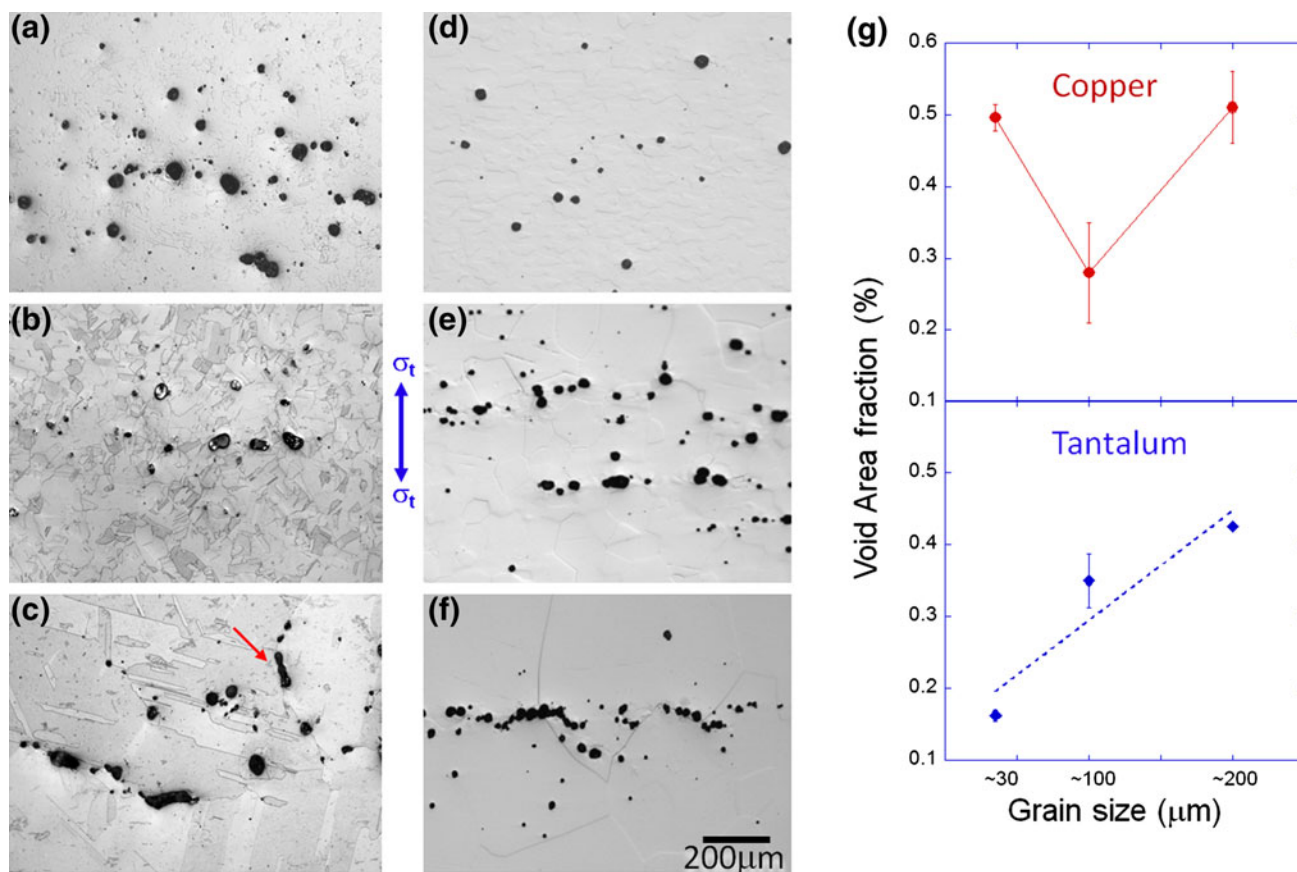


Fig. 3. Optical micrographs showing damage fields (voids) in copper: (a)  $\sim 30 \mu\text{m}$ , (b)  $\sim 100 \mu\text{m}$ , (c)  $\sim 200 \mu\text{m}$ ; and tantalum (d)  $\sim 35 \mu\text{m}$ , (e)  $\sim 85 \mu\text{m}$ , (f)  $\sim 200 \mu\text{m}$ . (g) Plot of the damage amount for Cu and Ta with varying grain size.

Philips, Amsterdam, the Netherlands) using a voltage of 20 kV, and a spot size of 4 with 1.5- $\mu\text{m}$  step size. Data were acquired and analyzed using orientation imaging microscopy (OIM) software by TexSEM Laboratories of EDAX (EDAX Inc., Mahwah, NJ, USA). The OIM software was used to calculate the properties obtained from EBSD measurements, such as orientation or Taylor Factor (TF) maps.

## RESULTS

Representative optical micrographs taken from the cross sections of the recovered samples for each

of the differently grain sized materials are shown in Fig. 3a–c for copper and Fig. 3d–f for tantalum. The shock direction was from bottom to top, i.e., the samples were pulled into tension ( $\sigma_t$ ) along the vertical axis as shown by the blue arrows. The amount of damage in the form of void area fraction ( $V_A$ ) was calculated by measuring the area of voids within the entire cross section of a recovered sample and divided by the total area of the section. The average values are listed in Table II and plotted in Fig. 3g.

The differences in the trend of the volume fraction of damage are easily appreciated for each material.

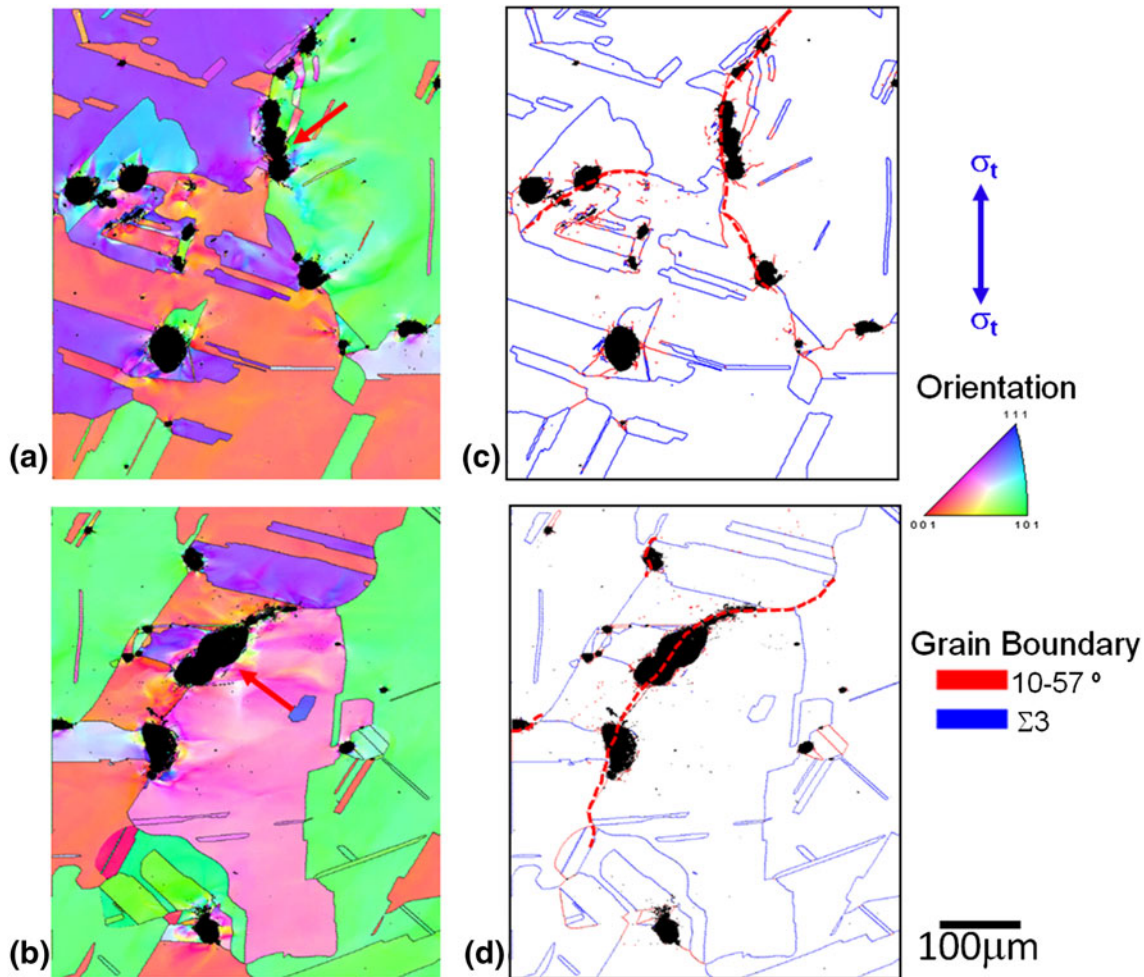


Fig. 4. (a, b) Orientation maps of selected areas in damaged copper samples and (c, d) respective boundary maps of the same areas. Special CSL  $\Sigma 3$  boundaries are colored as blue, and the general, low coincidence, high-angle ( $10^\circ$ – $57^\circ$ ) misorientation GBs are colored as red (Color figure online).

For copper, the volume fraction of damage is relatively high for small grain sizes; it decreases for intermediate grain size and increases again for the largest grain size tested. This is qualitatively observed in the optical micrographs and quantitatively measured in Fig. 3g. It should also be noted that this result was highly repeatable and well matched by three-dimensional tomographic statistics of the damage.<sup>18</sup> The void shape and size also differ as a function of grain size. While voids remain small and round for the intermediate grain size, they appear bigger and more elongated for the other two cases, indicating that more advanced stages of growth and coalescence have already begun. Furthermore, in the largest grain size material, it is easily observed that the voids tend to be aligned preferentially along the GBs, even if the GB is nearly parallel to the tensile axis as indicated by the arrow in Fig. 3c.

On the contrary, for tantalum the volume fraction of damage follows a nearly linear trend. An increasing amount of damage with increasing grain size is observed for the three microstructures tested

in this study. In addition, increasing grain size leads to an increasing amount of intergranular damage. For the case of the largest grain size, the voids seem to follow a path nearly perpendicular to the tensile axis (Fig. 3f).

To further assess differences in the damage evolution for the two materials, EBSD analyses were performed on the samples with the largest grain size. These microstructures allow for a careful examination of the damage fields near the GBs. High-magnification orientation fields maps of selected areas in damaged copper samples are shown in Fig. 4a and b. These micrographs confirm the optical observations that the voids preferentially sit along GBs. Coalescence of voids has become predominant with several small voids coalescing to render larger voids as signaled by the arrows in Fig. 4a and b. No clear correlation between grain orientations (grain color) and the location of the voids is observed. It has been reported that voids tend to predominately develop along boundaries with misorientation angles in the  $10^\circ$ – $57^\circ$  range,<sup>16,18</sup> whereas it seems that the boundaries

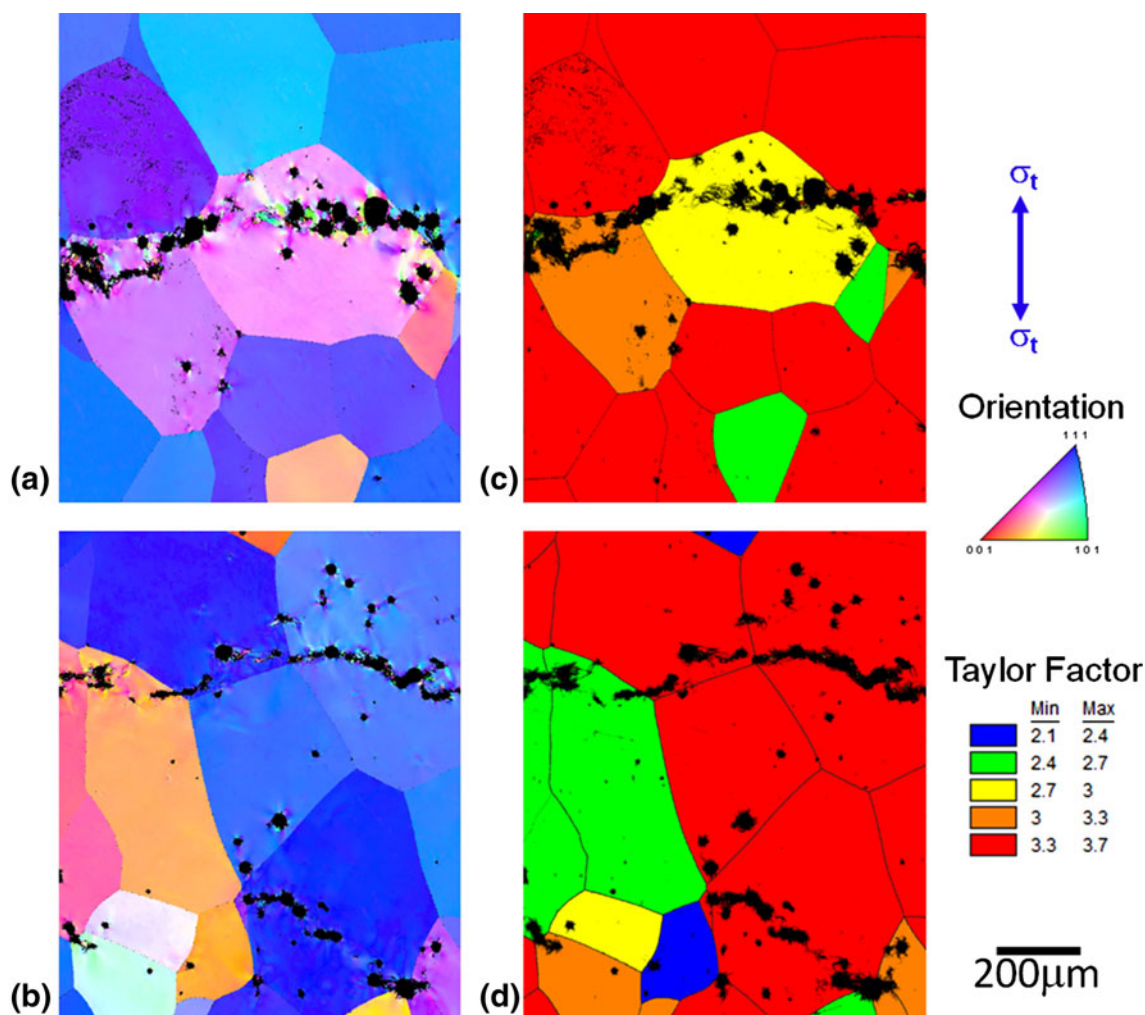


Fig. 5. (a, b) Orientation maps of selected areas in damaged tantalum samples. (c, d) Respective TF maps of the same areas. Intragranular void nucleation is not sensitive to TF, however early stage void coalescence seems to follow a preferential path.

with misorientation angle of  $\sim 60^\circ$ , corresponding to site-coincident  $\Sigma 3$  boundaries, seem to be less prone to void nucleation. As evidence of this phenomenon, Fig. 4c and d shows the grain boundary maps of the areas depicted in Fig. 4a and b, respectively. Colored in red are the GBs with misorientation angles between  $10^\circ$  and  $57^\circ$ , whereas colored blue are the  $\Sigma 3$  GBs. The aforementioned scenario for the location of voids is clearly appreciated in these images. Most of the voids lie along the red-colored boundaries. Noteworthy is the nearly null damage observed within grains.

Similar high-magnification orientation maps for damaged Ta samples are shown in Fig. 5a and b. It is clear that voids are not constrained to GBs as in the case of copper. A substantial amount of intergranular damage is observed in these micrographs. Also, there is no clear correlation between grain orientation and propensity to intergranular void formation. The TF maps are given in Fig. 5c and d. Voids are observed in many grains, irrespective of TF value. This finding is unexpected, as orientation

determines the propensity for plastic deformation, typically represented by the TF, normally seen as an important factor in void growth.<sup>29,30</sup> The results on this phenomenon have recently been reported for Cu, cavity growth and coalescence is promoted in relatively “soft” (low TF) grains, whereas hard grains (high TF) seem to hinder damage development.<sup>17,21</sup>

It is also interesting to note that coalescence of the voids seems to follow a semiwavy path nearly perpendicular to the tensile direction. Furthermore, these coalesced voids seem to align along specific directions within the grains, as shown in Fig. 5. To investigate this phenomenon, additional EBSD analyses were performed on selected grains. The Kernel misorientation maps in Fig. 6a and c confirm the development of voids and the accompanying plastic fields along specific directions. The lines in Fig. 6b and d are superimposed along the direction followed by the voids, and the respective arrows point to the normal of these directions. Through the use of pole figures, it was possible to assess the

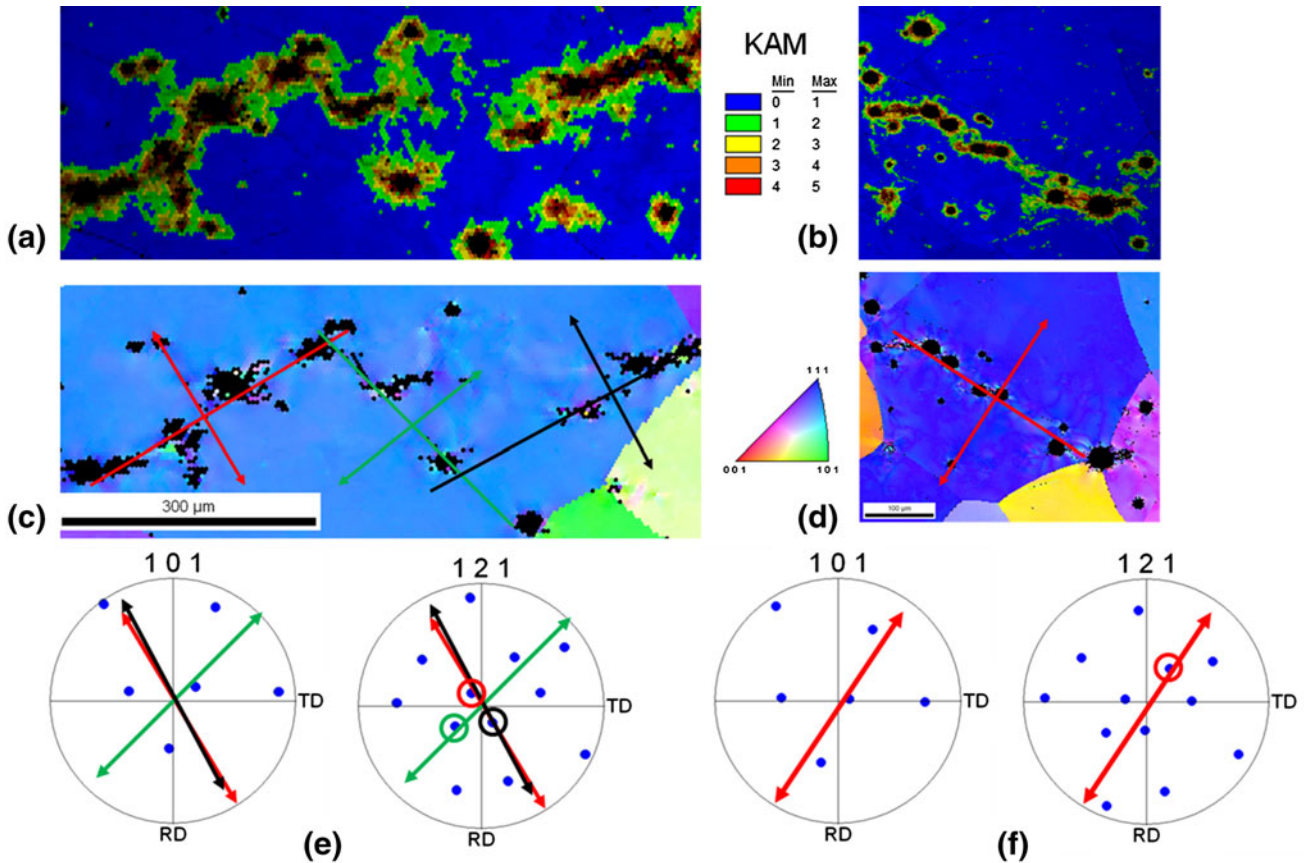


Fig. 6. (a, b) Kernel average misorientation (KAM) and orientation maps of selected grains in damaged tantalum samples. The arrows indicate the normal of the traces followed by the cavities. (c, d) Respective pole figures of the same areas showing the (101) and (121) poles, the primary slip planes in bcc materials. The arrows correspond to the same normals from the orientation maps. The preferential direction at which voids coalesce corresponds to  $\{121\}$  planes, as signaled by the colored circles (Color figure online).

preferential direction of such traces. As shown in Fig. 6c and d, the projected plane normals seem to align along the  $\langle 121 \rangle$  crystallographic directions. These results indicate that the voids develop along substructural features associated with  $\{121\}$  planes in bcc tantalum.

## DISCUSSION

Postimpact characterization of damaged copper and tantalum specimens allowed us to investigate the differences in damage development for each material. For the case of fcc copper, damage development was observed to follow a deterministic behavior: Voids preferentially nucleate, grow, and coalesce along general GBs with high misorientation angles, except for the  $\Sigma 3$  case. Experimental measurements<sup>17,20</sup> point to a lattice coherence between neighboring grains across GBs, which in turn provides for aligned slip systems in the adjacent grains. This likely allows for dislocation migration or secondary slip activation across the grains, therefore precluding dislocation pileups normally thought to contribute to stress concentrations required for void nucleation. In tandem, molecular

dynamic simulations have shown that shock-induced plasticity during the compressive stage increases the threshold in the stress necessary for void nucleation, which in turn increases the cohesive strength of  $\Sigma 3$  GBs.<sup>31</sup> These results collectively support the hypothesis that grain boundary structure plays a major role in the damage development process in fcc copper.<sup>8,9,16,32</sup>

On the contrary, in tantalum voids are observed to develop at GBs as well as within grains. Furthermore, these voids appear to follow a wavy path nearly perpendicular to the shock direction. Tonks et al.<sup>14</sup> reported on the reasons for this spatial waviness. The argument is that the plastic shock wave decomposes into wavelets that cause wavy plastic strains within the material. This process renders plastic fields following a wavy path across the specimen. Interestingly, the paths followed by the cavities and linking plastic fields in our samples lie along  $\{121\}$  planes. We propose that this preferential location likely arises due to the combination of three major deformation mechanisms occurring on these planes. First, dislocation cell walls have been observed to develop in shocked Ta.<sup>33–35</sup> Given that  $\{121\}$  planes are the preferred slip planes in bcc

materials, these dislocation walls tend to build at these specific planes. In addition, these planes also play a major role for twinning and omega transformation in polycrystalline Ta during shock loading.<sup>33,34</sup> Although the stresses employed in this study are well below the thresholds for such deformation mechanisms, 15 GPa and 45 GPa, respectively,<sup>33,34</sup> there is a tendency of enhanced shearing to occur on these planes under shock loading condition. Finally, a last contributor, for which extensive discussion is beyond the scope of this article, is the polarization of screw dislocation cores in bcc metals onto {121} planes under high-applied stresses.<sup>36,37</sup> Thus, the combination of intense shear, high degree of plastic deformation, and even dislocation core disassociation onto {121} planes makes these planes and their intersections with one another the most likely sites for transgranular void nucleation and growth, as presented experimentally in this article. Furthermore, it is possible that dislocation pileup initially occurred at the GBs, similar to copper. However, due to the abundance of possible slip systems in bcc Ta (48 in total), there is a high probability to find sets of aligned slip systems across GBs. This would allow for an easier dislocation transmission and/or secondary slip activation across GBs, shifting the location for damage development from GBs to the shock induced intragranular interfaces at the {121} planes.

### SUMMARY

This work examined the effect of crystalline structure on the early stages of dynamic damage evolution in shock-loaded Cu and Ta samples. The experiments were conducted at low stresses for the plate-impact technique as we aimed to examine the process of void nucleation, growth, and coalescence processes, which ultimately leads to intergranular failure. The experimental observations indicate that under the stress states investigated, damage in the form of voids preferentially develops along GBs in fcc copper. Specifically, this occurs at general or low coincidence, high-angle GBs, irrespective of grain size. On the contrary, the preferential location for damage shifts from GBs to intragranular damage in Ta. Specifically, damage occurs along subgranular interfaces associated with plastic processes occurring on the {121} planes. We propose that these additional sites for void nucleation in combination with an enhanced dislocation transmission/secondary slip system activation across GBs, due to the larger number of slip systems in bcc, are the likely factors responsible for the shift in the early stage damage mode from intergranular observed in fcc copper to intragranular observed in high-purity bcc tantalum.

### ACKNOWLEDGEMENTS

Los Alamos National Laboratory is operated by LANS, LLC, for the NNSA of the U.S. Department

of Energy under contract DE-AC52-06NA25396. Funding was provided by the LDRD-DR Grant 20100026.

### REFERENCES

1. L.E. Murr, *Shock Waves and High Strain Rate Phenomena in Metals*, ed. M.A. Meyers and L.E. Murr (New York: Plenum Press, 1981), p. 753.
2. T. Antoun, L. Seaman, D. Curran, G. Kanel, S. Razonerov, and A. Utkin, *Spall Fracture* (New York: Springer, 2002).
3. J.N. Johnson, *J. Appl. Phys.* 52, 2812 (1981).
4. D.R. Curran, L. Seaman, and D.A. Shockey, *Phys. Today* 30, 46 (1977).
5. G.T. Gray, *High Pressure Shock Compression of Solids*, ed. J.R. Asay and M. Shahinpoor (New York: Springer, 1993), p. 187.
6. L. Seaman, D.R. Curran, and D.A. Shockey, *J. Appl. Phys.* 47, 4814 (1976).
7. M.A. Meyers and C.T. Aimone, *Prog. Mater. Sci.* 28, 1 (1983).
8. T.A. Bamford, B. Hardiman, Z. Shen, W.A.T. Clark, and R.H. Wagoner, *Scripta Metall. Mater.* 20, 253 (1986).
9. J. Buchar, M. Elices, and R. Cortez, *J. Phys. IV* 1, 623 (1991).
10. J.N. Johnson, G.T. Gray, and N.K. Bourne, *J. Appl. Phys.* 86, 4892 (1999).
11. G.I. Kanel, *J. Appl. Mech. Tech. Phys.* 42, 358 (2001).
12. R.W. Minich, J.U. Cazamias, M. Kumar, and A.J. Schwartz, *Metall. Mater. Trans. A* 35A, 2663 (2004).
13. D.D. Koller, R.S. Hixson, G.T. Gray, P.A. Rigg, L.B. Addessio, E.K. Cerreta, J.D. Maestas, and C.A. Yablinsky, *J. Appl. Phys.* 98, 103518 (2005).
14. D.L. Tonks, B.L. Henrie, C.P. Trujillo, D. Holtkamp, and W.R. Thissell, *Shock Compress. Condens. Matter* 845, 670 (2006).
15. P. Peralta, S. DiGiacomo, S. Hashemian, S.N. Luo, D. Paisley, R. Dickerson, E. Loomis, D. Byler, and K.J. McClellan, *Int. J. Damage Mech.* 18, 393 (2009).
16. L. Wayne, K. Krishnan, S. DiGiacomo, N. Kovvali, P. Peralta, S.N. Luo, S. Greenfield, D. Byler, D. Paisley, K.J. McClellan, A. Koskelo, and R. Dickerson, *Scripta Mater.* 63, 1065 (2010).
17. J.P. Escobedo, E.K. Cerreta, D. Dennis-Koller, C.P. Trujillo, and C.A. Bronkhorst, *Philos. Mag.* 93, 833 (2013).
18. J.P. Escobedo, D. Dennis-Koller, E.K. Cerreta, B.M. Patterson, C.A. Bronkhorst, B.L. Hansen, D. Tonks, and R.A. Lebensohn, *J. Appl. Phys.* 110, 103513 (2011).
19. J.P. Escobedo, D. Dennis-Koller, E.K. Cerreta, and C.A. Bronkhorst, *American Institute of Physics Conference Proceedings*, vol. 1426, p. 1321 (2012).
20. E.K. Cerreta, J.P. Escobedo, A. Perez-Bergquist, D.D. Koller, C.P. Trujillo, G.T. Gray, C. Brandl, and T.C. Germann, *Scripta Mater.* 66, 638 (2012).
21. R.A. Lebensohn, J.P. Escobedo, E.K. Cerreta, D. Dennis-Koller, C.A. Bronkhorst, and J.F. Bingert, *Acta Mater.* 61, 6918 (2013).
22. L.M. Barker and Re Hollenba, *J. Appl. Phys.* 43, 4669 (1972).
23. W.F. Hemsing, *Rev. Sci. Instrum.* 50, 73 (1979).
24. O.T. Strand, D.R. Goosman, C. Martinez, T.L. Whitworth, and W.W. Kuhlow, *Rev. Sci. Instrum.* 77, 083108 (2006).
25. D. Dennis-Koller, J.P. Escobedo-Diaz, E.K. Cerreta, C.A. Bronkhorst, B. Hansen, R. Lebensohn, H. Mourad, B. Patterson, and D. Tonks, *American Institute of Physics Conference Proceedings*, vol. 1426, p. 1325 (2012).
26. W.R. Thissell, A.K. Zurek, D.A.S. Macdougall, and D. Tonks, *J. Phys. IV* 10, 769 (2000).
27. W.R. Thissell, A.K. Zurek, D.L. Tonks, and R.S. Hixson, *Shock Compress. Condens. Matter* 505, 451 (2000).
28. A.K. Zurek, W.R. Thissell, J.N. Johnson, D.L. Tonks, and R. Hixson, *J. Mater. Process Tech.* 60, 261 (1996).
29. V. Tvergaard and J.W. Hutchinson, *J. Mech. Phys. Solids* 40, 1377 (1992).



30. V. Tvergaard and J.W. Hutchinson, *Int. J. Solids Struct.* 39, 3581 (2002).
31. S.J. Fensin, S.M. Valone, E.K. Cerreta, J.P. Escobedo-Diaz, G.T. Gray, K. Kang, and J. Wang, *Model Simul. Mater. Sci.* 21, 015011 (2013).
32. J.P. Hirth, *Metall. Trans.* 3, 3047 (1972).
33. L.M. Hsiung and D.H. Lassila, *Scripta Mater.* 38, 1371 (1998).
34. L.M. Hsiung and D.H. Lassila, *Acta Mater.* 48, 4851 (2000).
35. J.C. Huang and G.T. Gray, *Acta Metall. Mater.* 37, 3335 (1989).
36. L.H. Yang, P. Soderlind, and J.A. Moriarty, *Mater. Sci. Eng. A* 309, 102 (2001).
37. L.H. Yang, P. Soderlind, and J.A. Moriarty, *Philos. Mag. A* 81, 1355 (2001).